Green Chemistry

PAPER

View Article Online
View Journal

Cite this: DOI: 10.1039/d5gc02628h

Biomimicry of CO_2 transfer through a biotin-mediated ATP-free pathway

Abdussalam K. Qaroush, *[a] Feda'a M. Al-Qaisi, *[b] Ala'a F. Eftaiha, *[b] Rana T. Abu-Saileek,[b] Khaleel I. Assaf,[c] Alex MacDonald[d] and Philip G. Jessop[a,b,d]

Received 26th May 2025,
Accepted 8th September 2025

DOI: 10.1039/d5gc02628h

rsc.li/greenchem

The *in vivo* bioprocess for the preparation of oxaloacetate from pyruvate is an energy-intensive process that depends on the reaction between the carbamimidic acid functionality of biotin and phosphorylated bicarbonate. In contrast, we report a *first-time* room-temperature approach that offers an *in vitro* alternative by exploiting the reactivity of the Mukaiyama-carbonic acid (MCA) adduct with biotin. Herein, the Mukaiyama reagent functions as an oxygen sink, bypassing the need for ATP-dependent phosphorylation and providing a benign pathway for biotin carboxylation under mild laboratory conditions, which facilitates CO_2 transfer to sodium pyruvate, leading to the formation of sodium oxaloacetate.

Green foundation

Our approach promotes the development of mild, energy-efficient, and sustainable synthetic strategies. By employing the Mukaiyama reagent as an oxygen sink, we enable CO_2 transfer from $NaHCO_3$ under ambient conditions. The resulting carbonic acid adduct facilitates biotin carboxylation without harsh reagents or high energy input, ultimately enabling the synthesis of sodium oxaloacetate from sodium pyruvate.

We utilized Mukaiyama reagent to activate CO_2 and transfer it to biotin under ATP-free conditions, forming a biotin carbamido–carboxylic acid adduct. This adduct was then used to carboxylate sodium 2-oxidoacrylate, yielding sodium oxaloacetate, demonstrating selective CO_2 transfer in a mild, energy-efficient system.

Greener alternatives could include aqueous or solvent-free conditions and catalytic MCA generation, reducing reagent use and minimizing waste.

1. Introduction

Biomimicry,[1] the imitation of nature's designs to solve global challenges, offers promising solutions for environmental sustainability in finding new energy efficient systems exploiting renewable resources as in CO_2 capture and utilization to make value-added products.[2–8] In this respect, readers are encouraged to refer to the review by Sarah Bierbaumer *et al.*, which provides a comprehensive framework for designing and implementing artificial carbon fixation pathways while highlighting examples of biocatalytic cascades involving carboxylases.[9]

For example, plants use photosynthesis to convert CO_2 and water into glucose,[10] while microorganisms capture CO_2 to produce methane or other organic compounds.[11] Humans capture and utilize CO_2 through various metabolic processes; in the body, CO_2 is initially converted into bicarbonate by carbonic anhydrase,[12] while biotin, acting as a coenzyme (Scheme 1A), plays a crucial role as a CO_2 transfer agent.[13] In the presence of magnesium and adenosine triphosphate (ATP), bicarbonate is transferred to biotin carboxylase, forming a carboxy–biotin complex. This complex subsequently transfers CO_2, *via* carboxyltransferase to form oxaloacetate,[2,14] which can participate in gluconeogenesis to produce glucose or contribute to fatty acid synthesis through citrate formation.[15,16] *In vitro*, thermodynamic constraints and strict biological conditions can be overcome by utilizing enzymatic pathways inspired by the CO_2 metabolism that occurs in cells.[17,18]

Understanding biotin's mechanism of action is crucial for mimicking its role in CO_2 fixation. *In vivo*, the enol tautomer of biotin carboxylase, carbamimidic acid, reacts with phosphorylated bicarbonate (Scheme 1A).[19] This ATP-driven process is essential for the subsequent carboxylation step, in which biotin acts as a carrier of activated carbon dioxide, transferring it to pyruvate to form the oxaloacetate (Scheme 1C). This reaction is a crucial step in gluconeogenesis.[19]

[a]*Department of Chemistry, Faculty of Science, The University of Jordan, 11942 Amman, Jordan. E-mail: a.qaroush@ju.edu.jo*
[b]*Department of Chemistry, Faculty of Science, The Hashemite University, Zarqa 13133, Jordan. E-mail: fedaam@hu.edu.jo, alaa.eftaiha@hu.edu.jo*
[c]*Department of Chemistry, Faculty of Science, Al-Balqa Applied University, Al-Salt 19117, Jordan*
[d]*Department of Chemistry, Queen's University, 90 Bader Lane, Kingston, Ontario, Canada K7L 2S8*

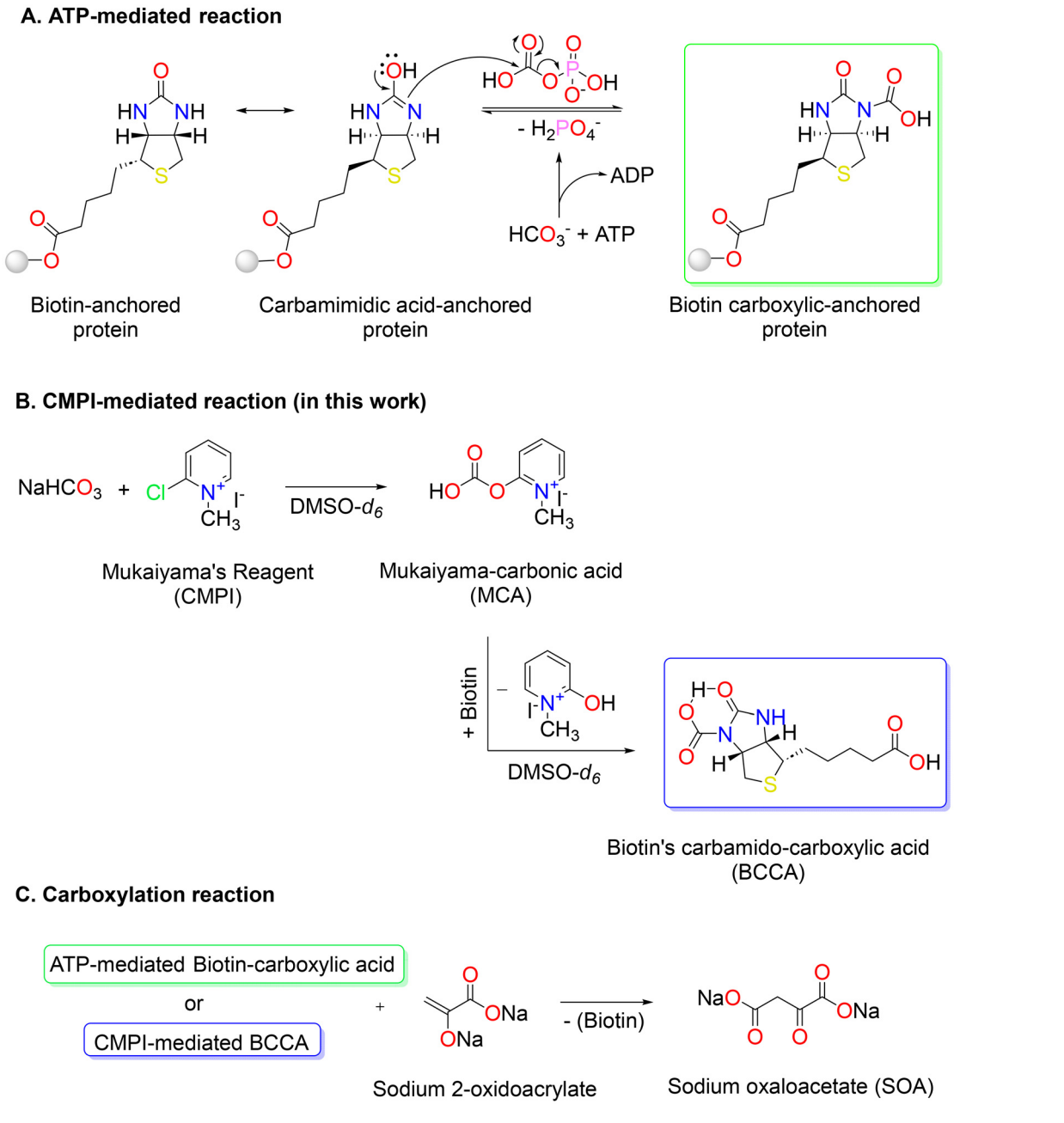

Scheme 1 A. Reaction mechanism of CO_2 transfer to biotin, forming biotin-carboxylic acid as a coenzyme.[2,14] B. The reaction of sodium bicarbonate as a C1-feedstock with 2-chloro-1-methylpyridinium iodide (CMPI) produces the Mukaiyama-carbonic acid (MCA) adduct, which subsequently reacts with biotin to form biotin's carbamido–carboxylic acid (BCCA), featuring a hydrogen atom between the two oxygen atoms that participates in an intramolecular hydrogen bond. This reaction is driven by CMPI, which functions as an oxygen-sink promoter. C. Conversion of sodium 2-oxidoacrylate to sodium oxaloacetate (SOA) through ATP- or CMPI-mediated formation of carboxylate/carboxylic biotin adducts.

To bypass the former energy penalty, our group has previously demonstrated the use of 2-chloro-1-methylpyridinium iodide, also known as the Mukaiyama reagent (CMPI), as an oxygen sink through a straightforward nucleophilic addition–elimination reaction.[20,21] In a prior study, a carbamate adduct, derived from ethylenediamine and CO_2, was reacted with CMPI under a nitrogen atmosphere, yielding cyclic urea and pyridone under basic conditions.[20] Additionally, CMPI was utilized to synthesize an ester-appended pyridine gemini surfactant from nicotinic acid and 1,4-benzenedimethanol.[21] These findings suggest that the oxygen removal step *via* bicarbonate phosphorylation can be accomplished using CMPI.

In this study, we utilized CMPI to transfer CO_2 into biotin under ATP-free conditions, to produce biotin carbamido–carboxylic acid adduct as shown in Scheme 1B, which was then employed to transfer CO_2 into sodium 2-oxidoacrylate, ultimately producing sodium oxaloacetate (Scheme 1C).

2. Results and discussion

2.1. Synthesis of Mukaiyama-carbonic acid (MCA) adduct

To achieve the postulated CO_2–biotin biomimicry in a controlled laboratory setting, we introduced a novel approach that bypasses traditional bicarbonate phosphorylation by transferring CO_2 to biotin using sodium bicarbonate ($NaHCO_3$) and CMPI, eliminating the need for ATP-dependent phosphorylation. As shown in Scheme 2, the reaction resulted in a petrol-colored precipitate, which we propose to be a Mukaiyama-carbonic acid (MCA) adduct, exists in equilibrium with CO_2 and the DMSO-soluble 2-hydroxy-1-methylpyridinium iodide (HMPI), highlighting its solubility in the reaction medium. As a side note, HMPI has previously been reported as the product of the reaction between 2-hydroxypyridine and methyl iodide. The resulting white solid was analyzed in DMSO.[22]

MCA was isolated by extensive washing with ethanol, then dissolved in D_2O and analyzed using ^1H and ^{13}C NMR spectroscopy. Fig. 1A shows that the ^{13}C NMR spectroscopy supports the formation of the MCA adduct through a downfield shift of the bicarbonate carbon from 160.6 (C-1) to 164.5 (C-1′) ppm.[23] Notably, the use of $NaH^{13}CO_3$ did not enhance the signal associated with C-1′, as shown in the spectrum provided in Fig. S5, indicating that the equilibrium proposed in Scheme 2 favors the formation of HMPI and CO_2. Further single crystal X-ray analysis for the needle crystals of MCA (prepared from either ethanol or DMSO) were not successful for the identification of the easy-to-prepare/isolate adduct.

Conducting the experiment under a CO_2 atmosphere enhanced the intensity of the 164.5 ppm peak by shifting the equilibrium toward the MCA adduct. This observation was consistent with the results obtained using $^{13}CO_2$, which also led to the appearance of

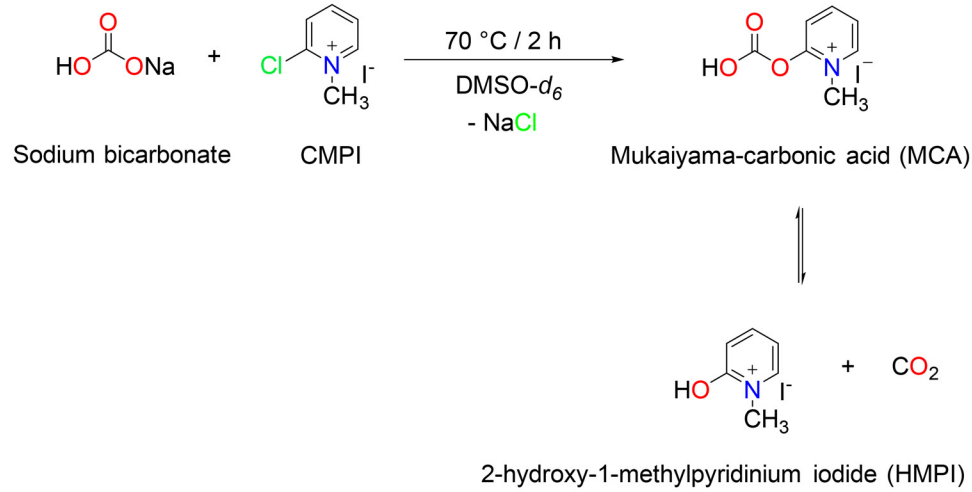

Scheme 2 The presumed structure of Mukaiyama-carbonic acid (MCA) adduct upon the reaction of sodium bicarbonate with CMPI. The ^1H and ^{13}C NMR spectra of the latter and HMPI, are provided in the Fig. S1–4.

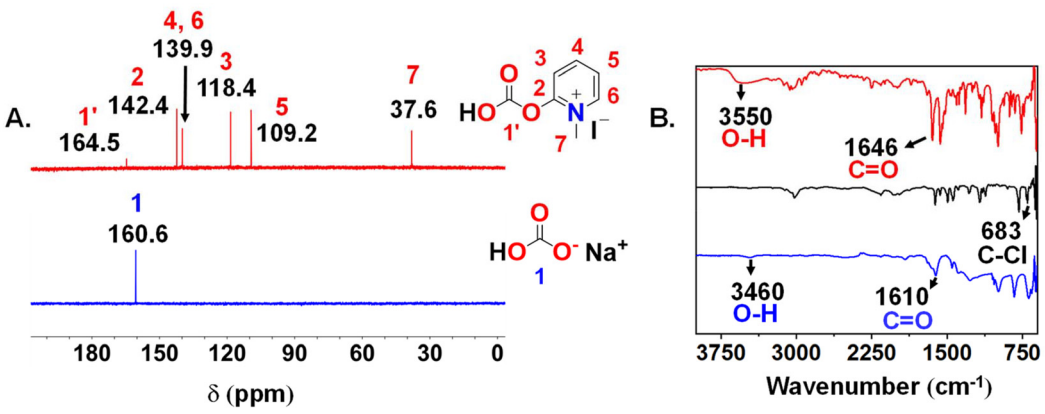

Fig. 1 A. Stacked ^{13}C NMR spectra of $NaHCO_3$ (blue trace) and the isolated MCA adduct (red trace), measured in D_2O. Note: although C-4 and C-6 of MCA are not chemically identical due to their different positions relative to the positively charged nitrogen, their electronic environments are nearly the same. This is attributed to their symmetrical placement with respect to the carboxylic acid group and the delocalization of the positive charge on the nitrogen, both of which contribute to the merging of their signals. B. *Ex situ* ATR-FTIR spectra (%transmittance *vs.* wavenumber) of the solid specimen of $NaHCO_3$ (blue trace), CMPI (black trace) and MCA adduct (red trace).

a peak at 124.8 ppm, corresponding to CO_2 dissolved in DMSO (Fig. S5). When the reaction was conducted under a CO_2 balloon, the yield of the MCA adduct increased substantially, from 35% to 94%. These observations can be explained by Le Chatelier's principle, where the excess CO_2 shifts the equilibrium between HMPI and CO_2 towards the formation of the MCA adduct. This was further verified by *ex situ* ATR-FTIR measurements of $NaHCO_3$, CMPI and the MCA adduct, both analyzed in their solid specimen form, as illustrated in Fig. 1B. The spectral data reveal that the asymmetric stretching vibration of the C═O group (likely associated with a dimeric bicarbonate ion) exhibits a pronounced blue shift from 1610 to 1646 cm^{-1} upon formation of the MCA adduct.[24,25] This is accompanied by the disappearance of the C–Cl stretching peak at 683 cm^{-1} and a shift in the –OH stretching band from 3460 to 3550 cm^{-1}.

The effect of temperature on the stability of the MCA adduct dissolved in DMSO was monitored using *in situ* ATR-FTIR spectroscopy by measuring changes in the intensity of the carboxylate peak at 1435 cm^{-1}. The adduct was prepared under optimized reaction conditions, as described in Section 4.3.1, and gradually heating between 70 and 150 °C. As shown in Fig. 2, increasing the temperature up to 150 °C resulted in a decrease in the intensity of the designated peak, as indicated by the horizontal-colored arrow. This behavior was attributed to the endothermic decomposition of MCA, where higher temperatures favour the forward reaction, leading to the formation of HMPI and CO_2, as presented in Scheme 2.

Interestingly, cooling the system back to 70 °C while introducing a CO_2 balloon led to an increase in the intensity of the peak, as highlighted by the vertical arrow (purple). This not only supported that the presence of CO_2 improves the reaction yield, as previously demonstrated in Section 2.1, but also validated the endothermic decomposition of the MCA adduct, with lower temperatures shifting the equilibrium toward adduct formation. In theory, the reaction between HMPI and CO_2 should produce

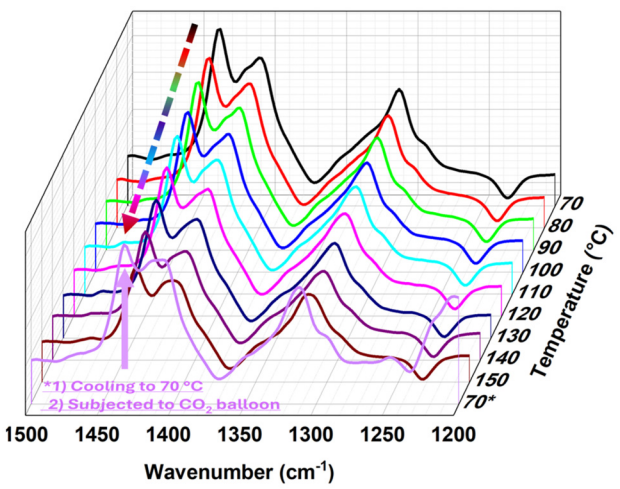

Fig. 2 3D *in situ* ATR-FTIR partial spectra (absorbance *vs.* wavenumber *vs.* temperature) of the MCA adduct dissolved in DMSO. The solution was heated from 70 to 150 °C, then cooled back to 70 °C before being exposed to CO_2 *via* a balloon.

MCA, but this would require the synthesis of HMPI, which is not commercially available and is beyond the scope of this work.

2.2. Synthesis of biotin's carbamido–carboxylic acid (BCCA) adduct

The reaction between biotin and MCA (obtained from the crude reaction mixture as described in Section 4.3.2) involved a nucleophilic attack by the nitrogen lone pair of biotin on the carboxylate group of the MCA adduct, leading to the formation of a carbamido–carboxylic acid (BCCA) adduct (Scheme 3).

This reaction likely proceeds with the elimination of 1-methylpyridinone and hydroiodic acid, possibly as HMPI, highlighting the role of CMPI as an oxygen sink by transferring oxygen to form the hydroxyl pyridinium species. Notably, using isolated MCA to carboxylate biotin, or synthesizing MCA at 70 °C, does not yield the BCCA adduct. While the latter precipitates as the reaction mixture cools to room temperature, the inability of isolated MCA to form the adduct suggests a potential role of HMPI, requiring further investigation.

BCCA was isolated as a white precipitate after a thorough washing of the reaction mixture with ethanol and diethyl ether. Its formation was confirmed by ^{13}C NMR spectroscopy in DMSO-d_6 (Fig. 3A), which revealed a chemical shift at 169.7 ppm, corresponding with the carbamido–carboxylic acid moiety. This finding was further confirmed by *ex situ* ATR-FTIR measurements (Fig. 3B), which indicated a blue shift of the MCA carboxyl group from 1685 to 1694 cm^{-1}, characteristic of the absorption bands associated with the BCCA adduct due to the formation of the carbamido–carboxylic acid functional group. This is in excellent agreement with the carboxylate asymmetric stretching vibration (coupled to the ureido carbonyl) reported by Clarkson and Carey.[26] Additionally, broadening of the O–H and N–H bands further supported the presence of hydrogen bonding. Moreover, high resolution mass spectrometry (HRMS) confirmed the formation of the BCCA adduct with an *m*/*z* of 289.05948 for the $[C_{11}H_{16}N_2O_5S]^+$ ion, which matched the calculated value of 289.05950.

2.3. Synthesis of sodium oxaloacetate (SOA)

Sodium pyruvate was activated with sodium hydride (NaH) and subsequently reacted with BCCA in its reaction mixture (as described in Section 4.3.2) to produce sodium oxaloacetate (SOA), as illustrated in Scheme 4.

The isolated SOA–biotin mixture (obtained by washing the reaction mixture with ethanol) was analyzed using ^{13}C NMR spectroscopy in D_2O as presented in Fig. 4. Upon the transfer of the carbonyl group from BCCA to sodium 2-oxidoacrylate, a downfield shift was observed at 171.5 ppm. Moreover, the chemical shift of the carbon labeled as "a" is down fielded from 26.3 to 37.3 ppm upon carboxylation. This observation was further supported by distortionless enhancement by polarization transfer at 135° (DEPT-135, Fig. S6) measurements, which confirmed the downward-pointing signal at 37.3 ppm, characteristic of the CH_2 carbon in SOA.

This reaction serves as a proof-of-concept to demonstrate the feasibility of chemically transferring CO_2 to sodium pyru-

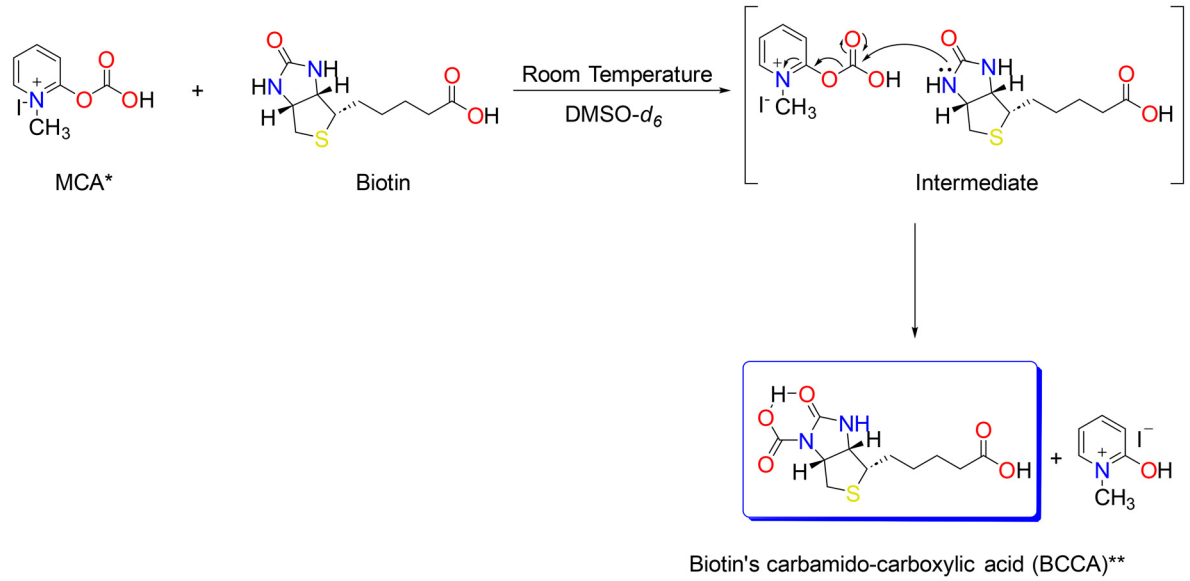

Scheme 3 Proposed reaction mechanism of MCA and biotin, leading to the carboxylation of biotin through the formation of the biotin carbamido–carboxylic acid (BCCA) adduct (which has been isolated and characterized) and the presumed production of 2-hydroxy-1-methylpyridinium iodide. *MCA was obtained from the crude reaction mixture as described in Section 4.3.2. **The hydrogen atom located between the two oxygen atoms participates in an intramolecular hydrogen bond resulting in proton shuttling.

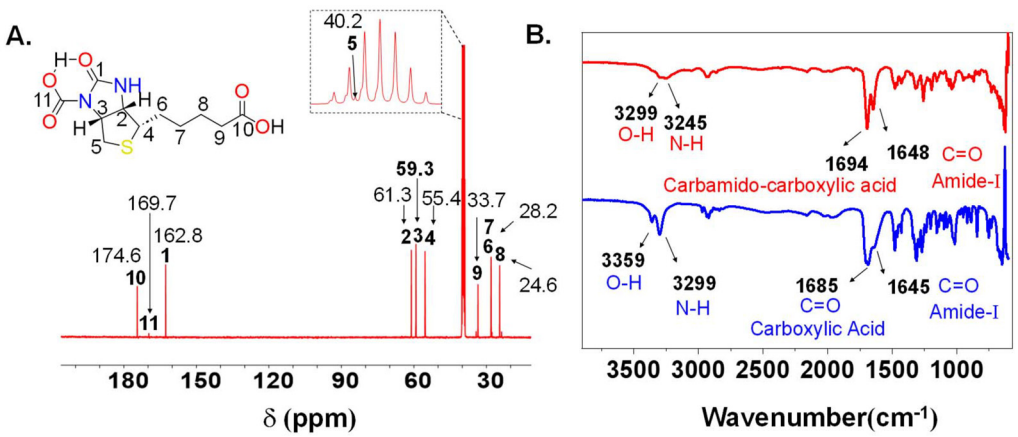

Fig. 3 A. ^{13}C NMR spectrum of BCCA adduct measured in DMSO-d_6, B. *Ex situ* ATR-FTIR spectra of biotin (blue trace), and BCCA adduct (red trace).

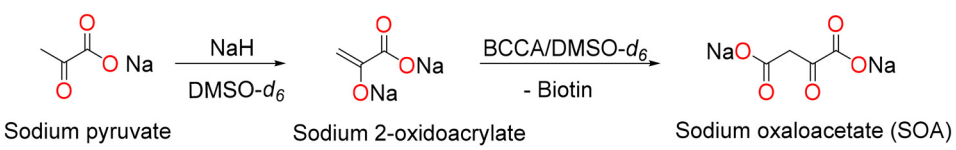

Scheme 4 Schematic representation of the synthesis of sodium oxaloacetate (SOA) from sodium 2-oxidoacrylate and BCCA. This reaction demonstrates the success of the employed biomimetic approach.

vate under mild laboratory conditions. While the product yield is currently low, this limitation highlights opportunities for optimization in future studies, such as improving reagent ratios, exploring alternative solvents, and optimizing temperature and reaction time.

We believe this approach has significant potential, as sodium pyruvate is only one representative substrate. Structurally related compounds such as acrylic acid, lactic acid, acetoacetic acid, levulinic acid, and cinnamic acid share key functional features, making them promising candidates

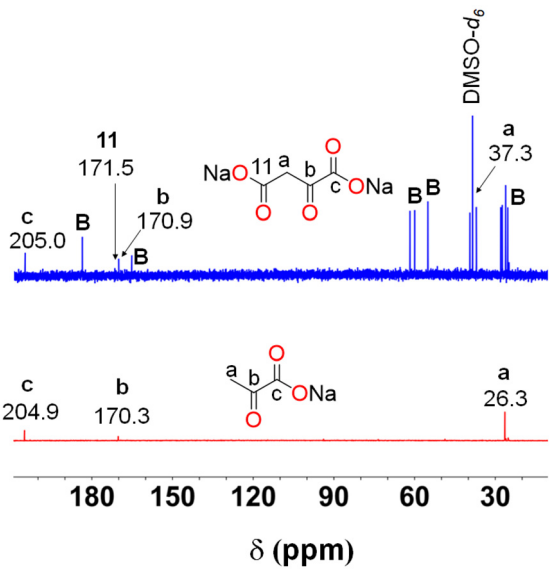

Fig. 4 ^{13}C NMR spectra of sodium pyruvate (red trace) and SOA (blue trace) measured in D_2O. **B**: labels corresponding to the biotin peaks. The carbon labeled as 11 in SOA corresponds to the carbon atom transferred from BCCA.

for further exploration. This suggests that the reaction can be extended to a broader range of substrates (bio-based or petroleum based), enabling the development of a versatile platform for CO_2 fixation into value-added organic compounds.

2.4. Theoretical calculations

The reaction mechanisms were further validated by density functional theory (DFT) calculations (Fig. 5). During the nucleophilic addition–elimination reaction between CMPI and bicarbonate ion, the calculated activation energy for the first transition state (TS_1) was relatively small value (5.7 kcal mol^{-1}). The structure of TS1 indicated that the oxygen atom of the bicarbonate ion was able to attack the electrophilic carbon of the CMPI, resulting in the elongation of the C–Cl bond (1.77 Å). Subsequently, the reaction proceeded with the elimination of the chloride ion and the formation of MCA adduct. The transfer of the carboxylic acid to biotin was further investigated using imidazloidin-2-one (as a model compound that mimics the structure of biotin). Initially, the nucleophilic nitrogen atom on the ureido group attacked the carbon atom of the carbonic functionality, a step which is associated by the elongation of C–O···COOH bond (from 1.36 to 1.74 Å). The reaction progressed through the second transition state (TS_2) with an activation energy of 13.0 kcal mol^{-1}. The overall stabilization energy for the latter step was found to be −18.5 kcal mol^{-1}.

3. Conclusion

In this study, we have demonstrated the role of CMPI in facilitating an unprecedented *in vitro* biotin-mediated carboxylation. By reacting with sodium bicarbonate, CMPI forms the MCA adduct, which enables CO_2 transfer to biotin, yielding its carbamido–carboxylic acid adduct (BCCA), with CMPI acting as an oxygen trap and promoter. Additionally, we have explored the role of BCCA in the conversion of sodium 2-oxidoacrylate to SOA. These findings offer new insights into pyridinium-based activation strategies for carboxylation reactions and hold promise for the efficient synthesis of valuable biochemicals and pharmaceuticals.

4. Experimental materials and methods

4.1. Chemicals

All chemicals were used without purification. Mukaiyama reagent (CMPI, 97%), sodium bicarbonate ($NaHCO_3$ and

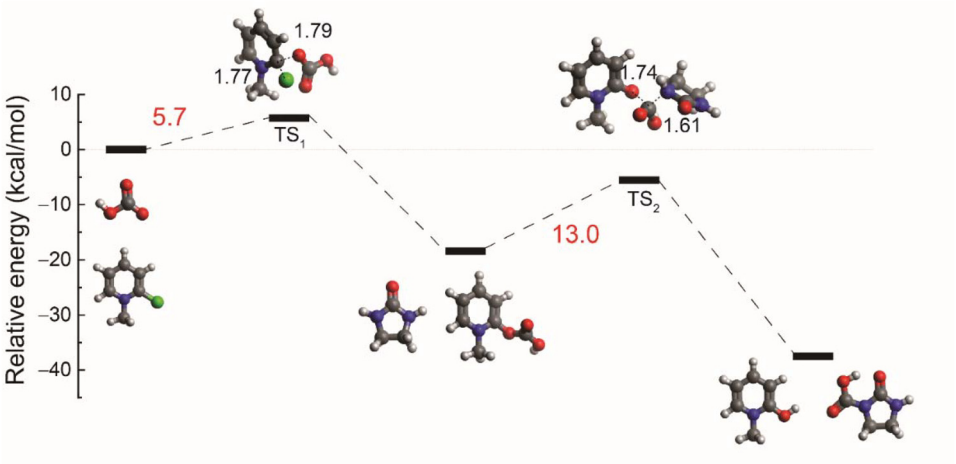

Fig. 5 Potential energy profile and optimized geometries of the nucleophilic addition–elimination reaction between CMPI and bicarbonate ion to produce the MCA adduct, followed by the production of carbamido–carbonic acid through the reaction of MCA and HMPI as a representative model compound. Bond distances are given in Å.

$NaH^{13}CO_3$ (99 atom% ^{13}C)), D(+)–biotin, sodium hydride (NaH, 60% dispersion in mineral oil), sodium pyruvate, dimethyl sulfoxide (DMSO-d_6, 99.5 atom% D), deuterium oxide (D_2O, 99.9 atom% D) and absolute ethanol were acquired from Sigma–Aldrich. N_2 (industrial grade) was purchased from Advanced Technical Gases Co. (Amman, Jordan).

4.2. Instrumentation

^1H and ^{13}C nuclear NMR spectra were measured using AVANCE-III 400 MHz (^1H: 400.13 MHz, ^{13}C: 100.61 MHz) equipped with a FTNMR Nano Bay spectrometer (Bruker, Switzerland). *Ex situ* ATR-FTIR spectra were recorded using a Bruker Vertex 70-FT-IR spectrometer at RT coupled with a Vertex Pt-ATR-FTIR accessory. *In situ* ATR-FTIR spectra were obtained using an INVENIO-R Bruker Optics fiber optic probe equipped with a ZnSe window. HRMS was performed using a quadrupole time-of-flight liquid chromatograph-mass spectrometer (LCMS-9050, Shimadzu).

4.3. Synthesis protocol

4.3.1. Synthesis of MCA. Under N_2 atmosphere, $NaHCO_3$ (34.4 mg, 0.41 mmol) was added to a solution of CMPI (100.0 mg; 0.41 mmol) dissolved in 1 mL of DMSO-d_6. The reaction mixture was stirred at 70 °C for 2 h, during which a color change from yellow to reddish brown was observed. The mixture was then allowed to stand at room temperature for 3 h, resulting in the formation of a petrol-colored precipitate. Finally, the precipitate was thoroughly washed with ethanol to remove 2-hydroxy-1-methylpyridinium iodide and dried under vacuum at room temperature for 24 h. The reaction yield was 35% (once a CO_2 balloon was used over the reaction, the MCA yield increased to 94%).

4.3.1.1. In situ ATR-FTIR measurements. In a round-bottom flask, $NaHCO_3$ was added to a solution of CMPI, as described previously, except that DMSO was used instead of the deuterated solvent. The mixture was stirred at 70 °C for 2 hours, after which the effect of temperature was monitored using *in situ* ATR-FTIR. The temperature was increased in 10 °C increments with the system stability allowance per 10 minutes at each step before recording the spectrum, up to a maximum of 150 °C. Subsequently, the temperature was lowered back to 70 °C, a CO_2 balloon was introduced, and the spectrum was recorded again.

4.3.2. One-pot synthesis of BCCA adduct (*in situ* procedure). Under N_2 atmosphere, $NaHCO_3$ (34.4 mg, 0.41 mmol) was added to a solution of CMPI (100.0 mg, 0.41 mmol) in 1 mL DMSO-d_6, and the reaction mixture was stirred at room temperature for 1 hour. A color change from yellow to reddish brown was observed. Biotin (0.41 mmol) was then added, and the mixture was stirred overnight at room temperature. The product was isolated by washing with copious amounts of ethanol and diethyl ether, yielding 37%. HRMS (m/z): $[C_{11}H_{16}N_2O_5S]^+$ (calculated: 289.05950, found: 289.05948).

4.3.3. Synthesis of SOA. Under N_2 atmosphere, sodium pyruvate (36.0 mg, 0.41 mmol) was deprotonated using sodium hydride (NaH, 60% in mineral oil, washed with hexane prior to use, 16.4 mg, 0.41 mmol) and stirred for 1 hour at room temperature to form the disodium salt. Subsequently, this was added to a solution of BCCA (obtained as in Section 4.3.2 prior to isolation) and stirred for 2 h to yield sodium oxaloacetate (SOA). The isolated SOA–biotin mixture was obtained by washing the reaction mixture with ethanol.

4.3.4. Density functional theory (DFT) calculations. DFT calculations were carried out using the Gaussian 16 software package, Revision C.02.[27] Geometry optimizations and energy calculations (including zero-point energy correction) were conducted with the M062X functional incorporating, and employing the 6-311++G** basis set. Solvent effects (DMSO) were incorporated using the implicit universal solvation model based on density (SMD).[28] Geometry optimizations were performed without structural constraints, and the global minima were confirmed through vibrational frequency calculations, yielding no negative eigenvalues for reactants and products, and one imaginary frequency for the transition states. Intrinsic reaction coordinate calculations were performed to support the structure of the transition states as shown in Fig. S7.

Author contributions

A. K. Q. and A. F. E. conceived the idea and methodology, guided data interpretation, and contributed to writing the manuscript. F. M. Q. established the methodology, led the experimental work and data interpretation, and contributed to manuscript writing. R. T. A. conducted the experimental work, prepared data presentations, and contributed to manuscript writing. K. I. A. performed the theoretical calculations, contributed to the methodology, guided data interpretation, and contributed to writing the manuscript. A. M. conducted the labeled CO_2 experiments. P. G. J. contributed to the methodology, participated in discussion of the results, and edited the manuscript.

Conflicts of interest

There are no conflicts to declare.

Data availability

The data supporting this article have been included as part of the SI. Supplementary information is available. See DOI: **https://doi.org/10.1039/d5gc02628h**.

Acknowledgements

A.K.Q., F.M.Q., and A.F.E. are thankful to the Scientific Research and Innovation Support Fund (SRISF), grant number (SE-WE/2/2024), for funding this work.

References

1 T. Rowley, *Lab. Anim.*, 2013, **42**, 271–272.
2 D. J. Heldebrant, J. Kothandaraman, N. M. Dowell and L. Brickett, *Chem. Sci.*, 2022, **13**, 6445–6456.
3 F. M. Al-Qaisi, A. K. Qaroush, A. H. Smadi, F. Alsoubani, K. I. Assaf, T. Repo and A. F. Eftaiha, *Dalton Trans.*, 2020, **49**, 7673–7679.
4 A. F. Eftaiha, A. K. Qaroush, F. Alsoubani, T. M. Pehl, C. Troll, B. Rieger, B. A. Al-Maythalony and K. I. Assaf, *RSC Adv.*, 2018, **8**, 37757–37764.
5 A. F. Eftaiha, F. M. Mustafa, F. Alsoubani, K. I. Assaf and A. K. Qaroush, *Chem. Commun.*, 2019, **55**, 3449–3452.
6 A. K. Qaroush, A. W. Alsayyed, A. F. Eftaiha, F. M. Al-Qaisi, K. I. Assaf, A. Y. Yousef and L. H. Idwaidar, *ACS Sustainable Chem. Eng.*, 2022, **10**, 15813–15823.
7 F. M. Al-Qaisi, A. K. Qaroush, I. K. Okashah, A. F. Eftaiha, P. Vasko, F. Alsoubani and T. Repo, *Eur. J. Inorg. Chem.*, 2023, **26**, e202200357.
8 F. M. Al-Qaisi, A. K. Qaroush, K. I. Assaf, A. F. Eftaiha, I. K. Okashah, A. H. Smadi, F. Alsoubani, A. S. Barham and T. Repo, *Inorg. Chim. Acta*, 2023, **557**, 121716.
9 S. Bierbaumer, M. Nattermann, L. Schulz, R. Zschoche, T. J. Erb, C. K. Winkler, M. Tinzl and S. M. Glueck, *Chem. Rev.*, 2023, **123**, 5702–5754.
10 J. A. Bassham and M. Calvin, in *Die CO_2-Assimilation/The Assimilation of Carbon Dioxide: In 2 Teilen/2 Parts*, ed. A. Pirson, Springer Berlin Heidelberg, Berlin, Heidelberg, 1960, pp. 884–922.
11 H. Salehizadeh, N. Yan and R. Farnood, *Chem. Eng. J.*, 2020, **390**, 124584.
12 J. Shi, Y. Jiang, Z. Jiang, X. Wang, X. Wang, S. Zhang, P. Han and C. Yang, *Chem. Soc. Rev.*, 2015, **44**, 5981–6000.
13 G. L. Waldrop, H. M. Holden and M. St. Maurice, *Protein Sci.*, 2012, **21**, 1597–1619.
14 J. A. Murillo-Lopez, N. Villegas-Escobar, S. Vogt-Geisse and E. Vöhringer-Martinez, *J. Phys. Chem. B*, 2024, **128**, 5327–5335.
15 D. J. Kelly and N. J. Hughes, in *Helicobacter pylori*, 2001, pp. 135–146.
16 M. Green, *J. Nutr.*, 2020, **150**, 2235–2238.
17 S. Talekar, B. H. Jo, J. S. Dordick and J. Kim, *Curr. Opin. Biotechnol.*, 2022, **74**, 230–240.
18 Y. Oku and T. Matsuda, *JACS Au*, 2024, **4**, 1758–1762.
19 T. Katagiri and Y. Amao, *Green Chem.*, 2020, **22**, 6682–6713.
20 A. K. Qaroush, A. F. Eftaiha, A. H. Smadi, K. I. Assaf, F. M. Al-Qaisi and F. Alsoubani, *ACS Omega*, 2022, **7**, 22511–22521.
21 A. F. Eftaiha, A. K. Qaroush, D. M. Foudeh, A. S. Aboshunnar, S. B. Hammad, K. I. Assaf and M. F. Paige, *Soft Matter*, 2024, **20**, 3742–3754.
22 A. Rostami, M. Mahmoodabadi, A. Hossein Ebrahimi, H. Khosravi and A. Al-Harrasi, *ChemSusChem*, 2018, **11**, 4262–4268.
23 S. Moret, P. J. Dyson and G. Laurenczy, *Dalton Trans.*, 2013, **42**, 4353.
24 K. Nakamoto, Y. A. Sarma and H. Ogoshi, *J. Chem. Phys.*, 1965, **43**, 1177–1181.
25 G. Busca and V. Lorenzelli, *Mater. Chem.*, 1982, **7**, 89–126.
26 J. Clarkson and P. R. Carey, *J. Phys. Chem. A*, 1999, **103**, 2851–2856.
27 M. J. Frisch, G. W. Trucks, H. B. Schlegel, G. E. Scuseria, M. A. Robb, J. R. Cheeseman, G. Scalmani, V. Barone, G. A. Petersson, H. Nakatsuji, X. Li, M. Caricato, A. V. Marenich, J. Bloino, B. G. Janesko, R. Gomperts, B. Mennucci, H. P. Hratchian, J. V. Ortiz, A. F. Izmaylov, J. L. Sonnenberg, D. Williams-Young, F. Ding, F. Lipparini, F. Egidi, J. Goings, B. Peng, A. Petrone, T. Henderson, D. Ranasinghe, V. G. Zakrzewski, J. Gao, N. Rega, G. Zheng, W. Liang, M. Hada, M. Ehara, K. Toyota, R. Fukuda, J. Hasegawa, M. Ishida, T. Nakajima, Y. Honda, O. Kitao, H. Nakai, T. Vreven, K. Throssell, J. A. Montgomery, Jr., J. E. Peralta, F. Ogliaro, M. J. Bearpark, J. J. Heyd, E. N. Brothers, K. N. Kudin, V. N. Staroverov, T. A. Keith, R. Kobayashi, J. Normand, K. Raghavachari, A. P. Rendell, J. C. Burant, S. S. Iyengar, J. Tomasi, M. Cossi, J. M. Millam, M. Klene, C. Adamo, R. Cammi, J. W. Ochterski, R. L. Martin, K. Morokuma, O. Farkas, J. B. Foresman and D. J. Fox, *Gaussian 16 (version Revision C.01)*, Gaussian, Inc., Wallingford CT, 2016.
28 A. V. Marenich, C. J. Cramer and D. G. Truhlar, *J. Phys. Chem. B*, 2009, **113**, 6378–6396.

